Inorg. Chem. **2009**, *48*, 55−67

Magnetic Frustration and Spin Disorder in Isostructural $M(\mu\text{-}OH_2)_2[Au(CN)_2]_2$ (M = Mn, Fe, Co) Coordination Polymers Containing Double Aqua-Bridged Chains: SQUID and μSR Studies

Julie Lefebvre,[†] Pooja Tyagi,[‡] Simon Trudel,[†,§] Vighen Pacradouni,[‡] Christina Kaiser,[‡] Jeff E. Sonier,[*,‡,||] and Daniel B. Leznoff[*,†]

Department of Chemistry, Department of Physics, and 4D LABS, Simon Fraser University, 8888 University Drive, Burnaby, British Columbia, Canada V5A 1S6, and Canadian Institute for Advanced Research, Toronto, Ontario, Canada M5G 1Z8

Received June 13, 2008

A series of isostructural $M(\mu\text{-}OH_2)_2[Au(CN)_2]_2$ (M = Co, Fe, and Mn) coordination polymers was synthesized from the reaction of M(II) with $[^nBu_4N][Au(CN)_2]$. The basic structural motif for these polymers is analogous to that of previously reported Cu(II)- and Ni(II)-containing polymers and contains repeating double aqua bridges between metal centers that yield a chain structure with pendant $[Au(CN)_2]^-$ units. The aqueous reaction with Fe(III) yields $Fe(\mu\text{-}OH_2)(\mu\text{-}OH)[Au(CN)_2]_2$, which has a similar structure. The magnetic properties of these polymers were investigated by a combination of SQUID magnetometry and zero-field muon spin relaxation. The double aqua bridges were found to mediate ferromagnetic interactions along the chains in the Co(II)-containing polymer, whereas intrachain antiferromagnetic interactions are present in the Fe(II)-, Fe(III)-, and Mn(II)-containing polymers. Weak magnetic interchain interactions mediated through hydrogen bonds, involving the bridging water molecules and the pendant cyanide groups, are also present. In zero field, the interchain interactions yield a phase transition to a disordered spin-frozen magnetic state below 2−5 K for every polymer. However, the degree of spin disorder varies considerably, depending on the metal center.

Introduction

Research in the field of coordination polymers has attracted attention due to the promise of generating materials with specific physical properties based on the chosen building blocks.[1] In particular, cyanometallate coordination polymers[2] have been targeted for their magnetic properties.[3] A wide range of magnetic behavior has been observed, including long-range magnetic ordering with Curie temperatures as high as 376 K,[4] photoinduced magnetism,[5] and room-temperature hysteretic spin-transition behavior.[6]

We recently reported on the structure and magnetic properties of two aqua-bridged cyanometallate coordination polymers of the form $M(\mu\text{-}OH_2)_2[Au(CN)_2]_2$ (M = Cu and Ni).[7] As shown in Figure 1, these polymers contain an unusual structural motif which consists of chains of metal

* Author to whom correspondence should be addressed. E-mail: dleznoff@sfu.ca (D.B.L.), jsonier@sfu.ca (J.E.S.).
† Department of Chemistry, Simon Fraser University.
‡ Department of Physics, Simon Fraser University.
§ 4D LABS, Simon Fraser University.
|| Canadian Institute for Advanced Research Toronto.

(1) (a) Ouahab, L. *Chem. Mater.* **1997**, *9*, 1909–1926. (b) Janiak, C. *J. Chem. Soc., Dalton Trans.* **2003**, 2781–2804. (c) Stuart, J. L. *Chem. Soc. Rev.* **2003**, *32*, 276–288. (d) Decurtins, S.; Pellaux, R.; Antorrena, G.; Palacio, F. *Coord. Chem. Rev.* **1999**, *190−192*, 841–854.
(2) Lefebvre, J.; Leznoff, D. B. In *Macromolecules Containing Metal and Metal-Like Elements*; Abd-El-Aziz, A. S., Carraher, C. E., Jr., Pittman, C. U., Jr., Zeldin, M., Eds.; Wiley-Interscience: New York, 2005; Vol. *5*, Chapter 7, pp 155−208.
(3) (a) Verdaguer, M.; Bleuzen, A.; Marvaud, V.; Vaissermann, J.; Seuleiman, M.; Desplanches, C.; Scuiller, A.; Train, C.; Garde, R.; Gelly, G.; Lomenech, C.; Rosenman, I.; Veillet, P.; Cartier, C.; Villain, F. *Coord. Chem. Rev.* **1999**, *190−192*, 1023–1047. (b) Ruiz, E.; Rodriguez-Fortea, A.; Alvarez, S.; Verdaguer, M. *Chem.−Eur. J.* **2005**, *11*, 2135–2144.
(4) (a) Hatlevik, O.; Buschmann, W. E.; Zhang, J.; Manson, J. L.; Miller, J. S. *Adv. Mater.* **1999**, *11*, 914–918. (b) Holmes, S. M.; Girolami, G. S. *J. Am. Chem. Soc.* **1999**, *121*, 5593–5594.
(5) (a) Sato, O.; Iyoda, T.; Fujishima, A.; Hashimoto, K. *Science* **1996**, *272*, 704–705. (b) Herrera, J. M.; Marvaud, V.; Verdaguer, M.; Marrot, J.; Kalisz, M.; Mathonière, C. *Angew. Chem., Int. Ed.* **2004**, *43*, 5468–5471.
(6) Bonhommeau, S.; Molnár, G.; Galet, A.; Zwick, A.; Real, J.-A.; McGarvey, J. J.; Bousseksou, A. *Angew. Chem., Int. Ed.* **2005**, *44*, 4069–4073.
(7) Lefebvre, J.; Callaghan, F.; Katz, M. J.; Sonier, J. E.; Leznoff, D. B. *Chem.−Eur. J.* **2006**, *12*, 6748–6761.

10.1021/ic801094m CCC: $40.75
Published on Web 11/21/2008

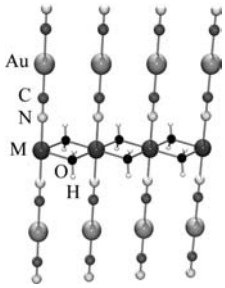

Figure 1. Structural motif of $M(\mu\text{-}OH_2)_2[Au(CN)_2]_2$ (M = Cu, Ni, Co, Fe, Mn), showing a chain formed by double aqua bridges.

centers bridged by two water molecules, with two trans pendant $[Au(CN)_2]^-$ groups.

Relative to the large number of reported oxo- and hydroxide-bridged dimers or oligomers,[8−10] very few aqua-bridged complexes are known. Magnetic studies on the Cu(II)- and Ni(II)-containing $M(\mu\text{-}OH_2)_2[Au(CN)_2]_2$ polymers revealed that weak ferromagnetic interactions are transmitted by the double aqua bridges along the chains. Also, through a combination of intra- and interchain interactions mediated through hydrogen bonding, the Cu(II)-containing polymer was found to magnetically order below 0.24 K while the Ni(II)-based polymer undergoes a transition to a disordered spin-frozen state below ~3.5 K.

In this context, we hereby report on the preparation and magnetic properties of the isostructural $M(\mu\text{-}OH_2)_2[Au(CN)_2]_2$ (M = Co, Fe, and Mn) and the related $Fe(\mu\text{-}OH_2)(\mu\text{-}OH)[Au(CN)_2]_2$ coordination polymers. In addition to superconducting quantum interference device (SQUID) magnetometry, the muon spin relaxation (μSR) technique was applied to obtain further information on the magnetic state of these polymers in zero applied field.[11] This technique[12] involves the implantation of nearly 100% spin-polarized positive muons into the sample. The implanted muon senses its magnetic environment via Larmor precession of its spin about the local magnetic field. This information is contained in the time evolution of the muon spin polarization $P_z(t)$, which is determined by detection of the decay positrons that are preferentially emitted along the direction of the muon spin. When relaxation of the ZF-μSR signal is observed, it indicates that there are static or dynamic random local magnetic fields.

Experimental Section

General Procedures and Physical Measurements. The reagents were purchased from commercial sources and used as received without further purification. $[^nBu_4N][Au(CN)_2]\cdot 0.5H_2O$ was prepared according to a previously reported synthesis.[13] Infrared spectra were recorded on a Thermo Nicolet Nexus 670 FTIR spectrometer with samples prepared as pressed KBr pellets. Microanalyses (C, H, N) were performed at Simon Fraser University using a computer-controlled Carlo Erba (Model 1106) CHN analyzer by Mr. M. K. Yang.

Synthesis of $Co(\mu\text{-}OH_2)_2[Au(CN)_2]_2$. A 15 mL acetonitrile solution of $[^nBu_4N][Au(CN)_2]\cdot 0.5H_2O$ (0.903 g, 1.81 mmol) was added to a 15 mL acetonitrile solution of $Co(ClO_4)_2\cdot 6H_2O$ (0.360 g, 0.984 mmol). An immediate pink precipitate was formed. The solution containing the precipitate was covered and left to sit overnight. The pink powder of $Co(\mu\text{-}OH_2)_2[Au(CN)_2]_2$ was collected the following day by filtration using a Buchner funnel and air-dried. Yield: 0.509 g, 94.9%. Anal. calcd for $C_4H_4N_4Au_2CoO_2$: C, 8.10; H, 0.68; N, 9.45. Found: C, 8.37; H, 0.77; N, 9.33. IR (KBr): 2204 (s), 2167 (s), 1530 (w), 1384 (w), 889 (w), 753 (w), 542 (w), 471 (w) cm^{-1}.

Synthesis of $Fe(\mu\text{-}OH_2)_2[Au(CN)_2]_2$. $[^nBu_4N][Au(CN)_2]\cdot 0.5H_2O$ (0.085 g, 0.17 mmol) was dissolved in 1 mL of a 98:2 acetonitrile/water mixture. $Fe(ClO_4)_2\cdot 6H_2O$ (0.036 g, 0.10 mmol) was then rapidly dissolved in 1 mL of the same solvent mixture, to which the $[Au(CN)_2]^-$ solution was immediately added while stirring. A pale yellow-peach precipitate was instantly formed. It was left to settle for 5 min and then filtered on a Buchner funnel, using all of the solution to wash the $Fe(\mu\text{-}OH_2)_2[Au(CN)_2]_2$ product. Yield: 0.037 g, 74%. Anal. calcd for $C_4H_4N_4Au_2FeO_2$: C, 8.14; H, 0.68; N, 9.50. Found: C, 8.34; H, 0.85; N, 9.41. IR (KBr): 2196 (s), 2165 (s), 1524 (w), 1094 (w), 877 (w), 747 (w), 535 (w) cm^{-1}. Shortly after drying, the powder was stored under nitrogen to prevent degradation.

Synthesis of $Mn(\mu\text{-}OH_2)_2[Au(CN)_2]_2$. A 6 mL acetonitrile solution of $[^nBu_4N][Au(CN)_2]\cdot 0.5H_2O$ (0.314 g, 0.627 mmol) was added to a 6 mL acetonitrile solution of $Mn(ClO_4)_2\cdot 6H_2O$ (0.116 g, 0.321 mmol). An immediate white precipitate was formed, and the powder of $Mn(\mu\text{-}OH_2)_2[Au(CN)_2]_2$ was collected by filtration, air-dried, and stored under a N_2 atmosphere. Yield: 0.163 g, 88%. Anal. calcd for $C_4H_4N_4Au_2MnO_2$: C, 8.16; H, 0.68; N, 9.51. Found: C, 8.33; H, 0.85; N, 9.28. IR (KBr): 2196 (w-m), 2161 (sh), 2158 (s), 1625 (w), 1518 (w), 1115 (w), 1090 (w), 859 (w), 741 (w), 527 (w), 460 (w) cm^{-1}. If left uncovered and exposed to the air, the powder was found to turn yellow or brown.

Synthesis of $Fe(\mu\text{-}OH_2)(\mu\text{-}OH)[Au(CN)_2]_2$. A 10 mL aqueous solution of $K[Au(CN)_2]$ (0.581 g, 2.02 mmol) was added dropwise to a 10 mL aqueous solution of $Fe(ClO_4)_3\cdot 6H_2O$ (0.359 g, 0.777 mmol). A very fine dark orange precipitate was formed immediately. The reaction mixture was transferred to a test tube and centrifuged for approximately 2−5 min. The overlying solution was then removed. To rinse the product and wash away any salt, water (10 mL) was added to the test tube and mixed with the precipitate. The mixture was centrifuged, after which the overlying solution was removed. The rinsing process was repeated two more times. After the final overlying solution was removed, the wet powder of $Fe(\mu\text{-}OH_2)(\mu\text{-}OH)[Au(CN)_2]_2$ was left to dry in the test tube. Yield: 0.305 g, 66.4%. Anal. calcd for $C_4H_3N_4Au_2FeO_2$: C, 8.16; H, 0.51; N, 9.51. Found: C, 8.13; H, 0.70; N, 9.47. IR (KBr): 2184 (s), 2168 (sh,s), 1612 (w), 669 (w), 518 (w) cm^{-1}.

Powder X-Ray Diffraction. Powder X-ray diffraction data for $M(\mu\text{-}OH_2)_2[Au(CN)_2]_2$ (M = Co, Mn) and $Fe(\mu\text{-}OH_2)(\mu$-

(8) Hatfield, W. E. *Magneto-Structural Correlations in Exchange Coupled Systems*; Reidel: Dordrecht, The Netherlands, 1984.
(9) Katz, M. J.; Shorrock, C. J.; Batchelor, R. J.; Leznoff, D. B. *Inorg. Chem.* **2006**, *45*, 1757–1765.
(10) Ruiz, E.; Alemany, P.; Alvarez, S.; Cano, J. *J. Am. Chem. Soc.* **1997**, *119*, 1297–1303.
(11) (a) Lancaster, T.; Blundell, S. J.; Pratt, F. L.; Coronado, E.; Galan-Mascaros, J. R. *J. Mater. Chem.* **2004**, *14*, 1518–1520. (b) Manson, J. L.; Lancaster, T.; Chapon, L. C.; Blundell, S. J.; Schlueter, J. A.; Brooks, M. L.; Pratt, F. L.; Nygren, L. C.; Qualls, J. S. *Inorg. Chem.* **2005**, *44*, 989–995. (c) Gatteschi, D.; Carretta, P.; Lascialfari, A. *Physica B* **2000**, *289*, 94–105. (d) Lancaster, T.; Blundell, S. J.; Pratt, F. L.; Brooks, M. L.; Manson, J. L.; Brechin, E. K.; Cadiou, C.; Low, D.; McInnes, E. J. L.; Winpenny, R. E. P. *J. Phys.: Condens. Matter* **2004**, *16*, S4563–S4582.
(12) Schenck, A. *Muon Spin Rotation Spectroscopy - Principles and Applications in Solid State Physics*; Adam Hilger Ltd.: Bristol, England, 1985.
(13) Lefebvre, J.; Chartrand, D.; Leznoff, D. B. *Polyhedron* **2007**, *26*, 2189–2199.

OH)[Au(CN)$_2$]$_2$ were collected by Dr. Brian O. Patrick (University of British Columbia, Canada) using a Bruker D8 Advance diffractometer equipped with a Cu sealed-tube source (powered at 40 kV and 40 mA), a graphite monochromator, and a scintillation detector. The diffractogram of the Fe(μ-OH$_2$)$_2$[Au(CN)$_2$]$_2$ complex was collected on a similar Bruker D8 Advance instrument at Simon Fraser University. Data were collected from 5 to 60° in 2θ by using a step of 0.02° and a total counting time of 3.9 s per step.

Indexing of the powder diffractograms was performed by using WinPLOTR[14] and DASH.[15] The simulation of powder diffractograms from atomic coordinates and comparison with experimentally obtained powder diffractograms were conducted by using POWDER CELL.[16]

Mössbauer Spectroscopy. ^{57}Fe Mössbauer spectra were acquired on a WEB Mössbauer spectroscopy system connected to a Janis Research variable-temperature SHI-850 Cryostat and a closed cycle refrigerator. A ^{57}Co (in rhodium matrix) source was used for the experiment. The γ-ray detector was a Reuters-Stokes Kr-CO$_2$ proportional counter. Each powdered sample (60−100 mg) was loaded in a 1 cm × 1 cm parafilm envelope, which was sealed with Kapton tape. The envelope was then fixed to the sample holder rod using Kapton tape. Mössbauer spectra were collected at 300 and 4.5 K in zero magnetic field. The velocity was scanned between −4 and +4 mm s^{-1}, using a constant acceleration triangle waveform. The spectra were calibrated against an Fe foil spectrum measured on the same instrument at 295 K in zero field. Fitting of the data was performed using the WMOSS software. The spectra were fit with a quadrupole-split pair of peaks, in which both peaks had the same area and line width.

SQUID Magnetometry. Magnetization measurements for each compound were performed on a Quantum Design MPMS-XL-7S SQUID magnetometer with an Evercool-equipped liquid helium dewar. Microcrystalline samples were packed in gelatin capsules and mounted in diamagnetic plastic straws. Direct current (dc) magnetization was measured for all samples upon cooling from 300 to 1.8 K under an applied dc field. The magnetic field was fixed at the following values for each compound: 1, 5, 10, 20, and 30 kOe for the Co-containing sample; 100 Oe, 1 kOe, and 5 kOe for the Fe(II)- and Mn(II)-containing samples; and 10 kOe for the Fe(III)-containing sample. The magnetization as a function of dc field strength (from 0 to 70 kOe) was also recorded at 1.8 K; in each case, the sample was first cooled from 100 K under zero applied field. The magnetic susceptibility of each compound was corrected for the diamagnetic contribution of the constituent atoms using Pascal's constants.[17]

The alternating current (ac) susceptibility of Co(μ-OH$_2$)$_2$-[Au(CN)$_2$]$_2$ was also determined in a zero applied dc field as a function of the temperature (100 to 1.8 K). The amplitude of the ac field was 5 Oe, and the frequency was varied between 1 and 1000 Hz.

***μ*SR Measurements.** The μSR experiments were performed using a dilution refrigerator on the M15 surface muon beam line at the TRI University Meson Facility (TRIUMF) in Vancouver, Canada. For each compound, two pressed polycrystalline pellets with masses ranging from 250 to 500 mg and a diameter of 1 cm were prepared and varnished onto a silver backing plate. The silver backing plate was then thermally anchored to the coldfinger of a ^{3}He/^{4}He dilution refrigerator. The arrangement of scintillation detectors used in the experiment was the same as previously reported.[7] The initial polarization, $P_z(0)$, was directed antiparallel to the beam momentum p_μ (i.e., along the z axis). The μSR measurements were taken both in zero external magnetic field (ZF) and in a longitudinal field (LF) geometry with the magnetic field applied parallel to $P_z(0)$.

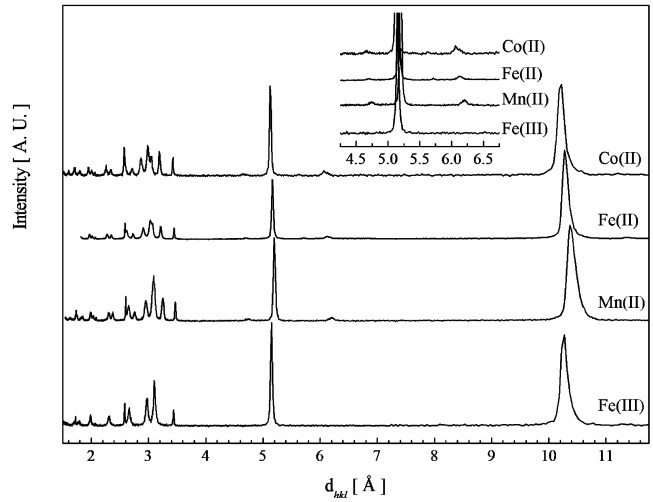

Figure 2. Comparison of the experimental powder X-ray diffractograms of M(μ-OH$_2$)$_2$[Au(CN)$_2$]$_2$ (M(II) = Co, Fe, Mn) and Fe(μ-OH$_2$)(μ-OH)[Au(CN)$_2$]$_2$ (Fe(III)). Inset shows a magnified view of the region between 4.5 and 6.5 Å.

Results

Synthesis of M(μ-OH$_2$)$_2$[Au(CN)$_2$]$_2$. The reaction of [^{n}Bu$_4$N][Au(CN)$_2$]·0.5H$_2$O with a series of M(ClO$_4$)$_2$·6H$_2$O salts in either acetonitrile (M = Co, Mn) or an acetonitrile/water mixture (M = Fe) afforded immediate precipitates of M(μ-OH$_2$)$_2$[Au(CN)$_2$]$_2$. Each product was found to have two bands in its FT-IR spectrum attributable to cyanide vibrations at ∼2200 and ∼2170 cm^{-1}; these are shifted toward higher energy relative to the stretching frequency for K[Au(CN)$_2$] (2141 cm^{-1}). This shift suggests that the cyanide groups are N-bound to the transition metal centers or hydrogen-bonded to the water molecules.[18]

Structure Determination for M(μ-OH$_2$)$_2$[Au(CN)$_2$]$_2$. The powder X-ray diffractogram of each M(μ-OH$_2$)$_2$-[Au(CN)$_2$]$_2$ (M(II) = Co, Fe, Mn) complex was measured and is shown in Figure 2. All of the measured diffractograms show the same basic features, with similar peak positions and relative intensities. A slight shift toward larger d_{hkl} values can be observed for the Mn(II)-containing complex compared to the other complexes. These powder X-ray diffractograms are very similar to those of the previously reported Ni(μ-OH$_2$)$_2$[Au(CN)$_2$]$_2$ and Cu(μ-OH$_2$)$_2$[Au(CN)$_2$]$_2$ coordination polymers[7] and can be indexed to similar or related unit cells (Table 1). This suggests that the arrangement of the building blocks is similar in all M(μ-OH$_2$)$_2$[Au(CN)$_2$]$_2$ complexes (M(II) = Cu, Ni, Co, Fe, Mn).

Structural models, whose calculated diffractograms match well with the experimentally obtained ones (Figures S1−S3,

(14) Roisnel, T.; Rodriguez-Carvajal, J. *Proceedings of the Seventh European Powder Diffraction Conference (EPDIC 7)*, Barcelona, Spain, May 20−23, 2000; pp 118−123.
(15) David, W. I. F.; Shankland, K.; van de Streek, J.; Pidcock, E.; Motherwell, W. D. S.; Cole, J. C. *J. Appl. Crystallogr.* **2006**, *39*, 910–915.
(16) Kraus, W.; Nolzeb, G. *J. Appl. Crystallogr.* **1996**, *29*, 301–303.
(17) Kahn, O., *Molecular Magnetism*; VCH: Weinheim, Germany, 1993.
(18) Dunbar, K. R.; Heintz, R. A. *Prog. Inorg. Chem.* **1997**, *45*, 283–391.

Table 1. Unit Cell Parameters for the M(μ-OH_2)$_2$[Au(CN)$_2$]$_2$ (M(II) = Cu, Ni, Co, Fe and Mn) and Fe(μ-OH_2)(μ-OH)[Au(CN)$_2$]$_2$ (Fe(III)) Complexes

	Cu(II)[a]	Ni(II)[a,b]	Co(II)	Fe(II)	Mn(II)	Fe(III)
crystal system	monoclinic	orthorhombic	monoclinic	monoclinic	monoclinic	orthorhombic
space group	*P*2 or *P*2/*m*	*Immm*	*P*2/*m*	*P*2/*m*	*P*2/*m*	*Cmmm*
a, Å	6.335	6.374(3)	6.40	6.43	6.50	6.26
b, Å	20.509	3.3183(11)	20.61	20.67	20.78	3.59
c, Å	3.482	20.512(5)	3.39	3.47	3.49	10.34
β, deg	90.93	90.0	90.48	90.68	90.4(3)	90.0
volume, Å^3	452.32	433.9(3)	446.99	460.32	471.38	231.98

[a] From ref 7. [b] From single-crystal data.

Supporting Information) were generated for each compound using the indexed unit cell parameters and atomic coordinates similar to those of Cu(μ-OH_2)$_2$[Au(CN)$_2$]$_2$ (Tables S1−S3, Supporting Information). The positions of the oxygen atoms and their associated hydrogen atoms could not be determined accurately, as they do not affect the diffractograms to a great extent.

Different Synthetic Routes. The preparation method for the Co(II)-, Fe(II)-, and Mn(II)-containing M(μ-OH_2)$_2$-[Au(CN)$_2$]$_2$ polymers differs from the aqueous synthesis reported for the analogous Cu(II) and Ni(II) polymers in that the aqueous reactions involving Co(II), Fe(II), and Mn(II) salts with K[Au(CN)$_2$] yield different products. For example, the aqueous reaction of Fe(ClO$_4$)$_2$·6H$_2$O with K[Au(CN)$_2$] was previously reported[19] and affords a coordination polymer with a different chemical composition, K{Fe[Au(CN)$_2$]$_3$}, irrespective of the Fe(II)/[Au(CN)$_2$]$^-$ ratio in solution. The similar aqueous reaction between Mn(ClO$_4$)$_2$·6H$_2$O and K[Au(CN)$_2$] was reported[19] to form Mn[Au(CN)$_2$]$_2$(H$_2$O)$_2$, a polymorph of Mn(μ-OH_2)$_2$[Au(CN)$_2$]$_2$. The structure of Mn[Au(CN)$_2$]$_2$(H$_2$O)$_2$ consists of square grid arrays of Mn[Au(CN)$_2$]$_2$ with nonbridging water molecules bound to the Mn(II) centers in a trans fashion on each side of the grids. The aqueous reaction of Co(ClO$_4$)$_2$·6H$_2$O with K[Au(CN)$_2$], on the other hand, yielded a mixture of [Au(CN)$_2$]-containing products that could not be separated. The aqueous syntheses of both Co[Au(CN)$_2$]$_2$[20] and K{Co[Au(CN)$_2$]$_3$}[21] were previously reported, and these products could be present in the mixture obtained. In all cases, a change in solvent, from water to acetonitrile, allowed a pure product to be obtained.

An Uncommon Motif. The repeating double aqua-bridge motif adopted by the M(μ-OH_2)$_2$[Au(CN)$_2$]$_2$ (M = Cu, Ni, Co, Fe and Mn) coordination polymers is very rare in coordination chemistry, irrespective of the identity of the metal center. Only a small number of isolated mono or doubly aqua-bridged dimers are known for each type of metal center: Co(II),[22,23] Fe(II),[22,24] and Mn(II).[22,25] In most cases, a second ligand, often a carboxylate group, is bridging the metal centers in addition to the water molecules. M(μ-OH_2)$_2$M units have also been observed in the 3-D framework of Mn$_2$[Ru(CN)$_6$]·8H$_2$0,[26] as well as the cluster-containing [Co$_2$(H$_2$O)$_4$][Re$_6$S$_8$(CN)$_6$]·10H$_2$O and [Co(H$_2$O)$_3$]$_4$[Co$_2$-(H$_2$O)$_4$][Re$_6$S$_8$(CN)$_6$]$_3$·44H$_2$O coordination polymers.[27]

Fe(μ-OH_2)(μ-OH)[Au(CN)$_2$]$_2$. When an aqueous solution of Fe(ClO$_4$)$_3$·6H$_2$O was mixed with a solution of K[Au(CN)$_2$], an immediate deep orange precipitate of Fe(μ-OH_2)(μ-OH)[Au(CN)$_2$]$_2$ was obtained. The FT-IR spectrum of this product showed two poorly resolved bands, at 2184 and 2168 cm^{-1}, attributable to cyanide stretching vibrations. Hydrolysis of [Fe(H$_2$O)$_6$]$^{3+}$ to produce [Fe(H$_2$O)$_5$(OH)]$^{2+}$ is known to occur in aqueous solution[28] and would explain the presence of hydroxide units. From the formation constant ($K = 10^{-3.05}$), it can be expected that [Fe(H$_2$O)$_5$(OH)]$^{2+}$ will form unless the solution is very acidic.

The powder X-ray diffractogram of Fe(μ-OH_2)(μ-OH)[Au(CN)$_2$]$_2$ was found to have similar features to that of the M(μ-OH_2)$_2$[Au(CN)$_2$]$_2$ coordination polymers (Figure 2). However, the low-intensity peaks at around 4.65 and 6.15 Å are absent in Fe(μ-OH_2)(μ-OH)[Au(CN)$_2$]$_2$ (Figure 2 inset). The diffractogram of Fe(μ-OH_2)(μ-OH)[Au(CN)$_2$]$_2$ can be indexed to a few unit cells with dimensions related to those of M(μ-OH_2)$_2$[Au(CN)$_2$]$_2$. Among the best possibilities, an orthorhombic unit cell (Table 1) was obtained with the same *a* and *b* parameters as Ni(μ-OH_2)$_2$[Au(CN)$_2$]$_2$ but with a *c* parameter 50% smaller.

A general structural model, which predicts all of the features observed experimentally, is proposed and shown in Figure 3A. The basic structural motif of M(μ-OH_2)$_2$[Au(CN)$_2$]$_2$, that is, M−(O)$_2$−M bridges, is also present in this structure. However, in this unit cell, the Fe(III) and oxygen atoms occupy an additional crystallographic site, with a half-occupancy on each site; it is assumed that, when an Fe(III) center is absent, the associated oxygen atoms are also absent and vice versa. The half-occupancies imply that the structure of Fe(μ-OH_2)(μ-OH)[Au(CN)$_2$]$_2$ does not contain infinite chains like the M(μ-OH_2)$_2$[Au(CN)$_2$]$_2$ polymers, but that M−NCAuCN−M fragments are also present. The structure can be considered as consisting of a random mixture of the sheets and chains substructures shown in Figure 3B

(19) Dong, W.; Zhu, L.-N.; Sun, Y.-Q.; Liang, M.; Liu, Z.-Q.; Liao, D.-Z.; Jiang, Z.-H.; Yan, S.-P.; Cheng, P. *Chem. Commun.* **2003**, 2544–2545.

(20) Abrahams, S. C.; Zyontz, L. E.; Bernstein, J. L. *J. Chem. Phys.* **1982**, *76*, 5458–5462.

(21) Abrahams, S. C.; Bernstein, J. L.; Liminga, R. *J. Chem. Phys.* **1980**, *73*, 4585–4590.

(22) Coucouvanis, D.; Reynolds, R. A., III; Dunham, W. R. *J. Am. Chem. Soc.* **1995**, *117*, 7570–7571.

(23) (a) Lee, D.; Hung, P.-L.; Spingler, B.; Lippard, S. J. *Inorg. Chem.* **2002**, *41*, 521–531. (b) Meng, X.; Hou, H.; Li, G.; Ye, B.; Ge, T.; Fan, Y.; Zhu, Y.; Sakiyama, H. *J. Organomet. Chem.* **2004**, *689*, 1218–1229. (c) Brown, D. A.; Glass, W. K.; Fitzpatrick, N. J.; Kemp, T. J.; Errington, W.; Müller-Bunz, H.; Hussein, A. J.; Nimir, H. *Inorg. Chim. Acta* **2005**, *358*, 2755–2762.

(24) Yoon, S.; Lippard, S. J. *J. Am. Chem. Soc.* **2004**, *126*, 16692–16693.

(25) Ghosh, S. K.; Ribas, J.; El Fallah, M. S.; Bharadwaj, P. K. *Inorg. Chem.* **2005**, *44*, 3856–3862.

(26) Rüegg, M.; Ludi, A.; Rieder, K. *Inorg. Chem.* **1971**, *10*, 1773–1777.

(27) Beauvais, L. G.; Shores, M. P.; Long, J. R. *J. Am. Chem. Soc.* **2000**, *122*, 2763–2772.

(28) Cotton, F. A.; Wilkinson, G. Advanced Inorganic Chemistry, 2nd ed.; Interscience Publishers: New York, 1966.

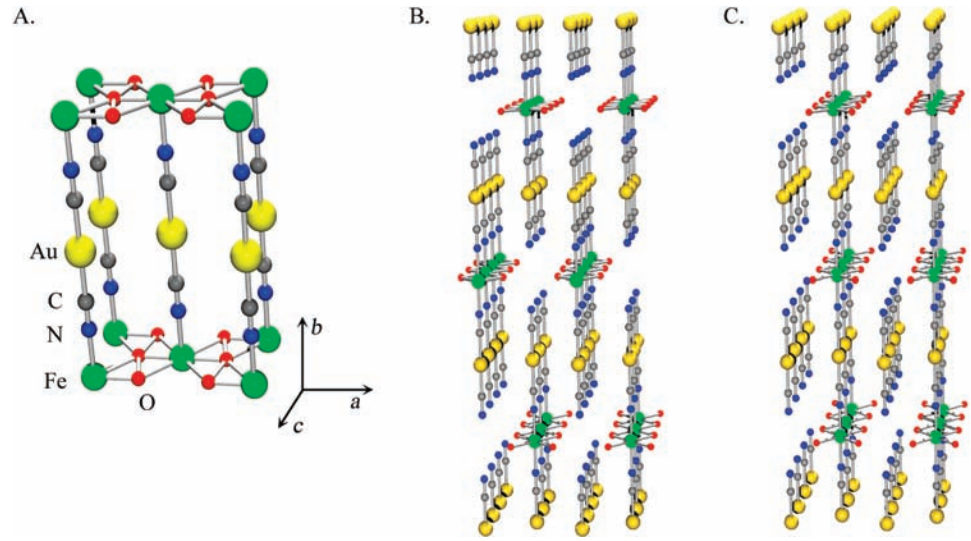

Figure 3. (A) Unit cell proposed for Fe(μ-OH_2)(μ-OH)[$Au(CN)_2]_2$ in which the Fe(III) and oxygen atoms have a half-occupancy. (Hydrogen atoms are not shown.) Two possible motifs, ribbon (B) vs sheet model (C), generated by the half-occupancy of the Fe(III) and O atoms.

and C. In other words, defects are present along the chains, and chain fragments are connected by $[Au(CN)_2]^-$ units to form partial sheets.

In this model, the hydroxide and water groups act as bridging ligands between the Fe(III) centers. These two groups could be randomly distributed along the structure or could alternate in a regular pattern (i.e., either aqua-hydroxo bridges, Fe(μ-OH_2)(μ-OH)Fe, or double aqua bridges alternating with double hydroxo bridges, Fe(μ-$OH)_2$Fe(μ-$OH_2)_2$Fe), but there is no experimental evidence to distinguish between these different situations.

The atomic coordinates for Fe(μ-OH_2)(μ-OH)[$Au(CN)_2]_2$ are reported in Table S4 (Supporting Information). As was the case for the M(μ-$OH_2)_2$[$Au(CN)_2]_2$ coordination polymers, the position of the oxygen atoms could not be accurately determined.

Some examples of the aqua-hydroxo bridging motif, proposed to be present in Fe(μ-OH_2)(μ-OH)[$Au(CN)_2]_2$, have been reported with different transition metal centers. To our knowledge, however, only one example of an Fe(II) dimer with an aqua-hydroxo bridging motif can be found in the literature,[29] and no Fe(III)-containing dimer or polymer with this bridge is known.

Mössbauer Spectroscopy. To confirm the oxidation state and assess the spin configuration of the Fe centers in the two Fe-containing complexes, ^{57}Fe Mössbauer spectroscopy was performed.

Figure 4A shows the Mössbauer spectrum of Fe(μ-$OH_2)_2$[$Au(CN)_2]_2$ collected at 4.5 K. A quadrupole-split doublet is observed, with an isomer shift (δ) of 1.25(2) mm s^{-1} and a quadrupole splitting (ΔE_Q) of 2.98(2) mm s^{-1}. These values indicate the presence of high-spin Fe(II) centers in Fe(μ-$OH_2)_2$[$Au(CN)_2]_2$.[30]

The Mössbauer spectrum acquired at 4.5 K for Fe(μ-OH_2)(μ-OH)[$Au(CN)_2]_2$ is shown in Figure 4B. A quadrupole-split doublet with an isomer shift (δ) of 0.47(3) mm

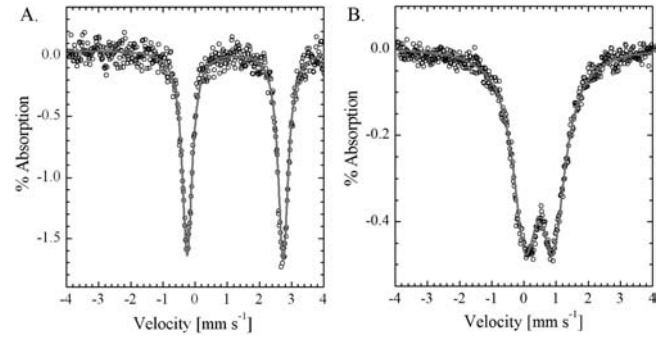

Figure 4. Mössbauer spectra of Fe(μ-$OH_2)_2$[$Au(CN)_2]_2$ (A) and Fe(μ-OH_2)(μ-OH)[$Au(CN)_2]_2$ (B) acquired at 4.5 K. Solid lines correspond to the envelope of the fit.

s^{-1} and a ΔE_Q of 0.88(3) mm s^{-1} can be observed. These values are typical for paramagnetic high-spin Fe(III) centers.[30]

For both products, no additional peaks were present in the Mössbauer spectrum, which confirms the presence of only one type of Fe center per compound.

Magnetic Properties by SQUID Magnetometry. The magnetization of each M(μ-$OH_2)_2$[$Au(CN)_2]_2$ polymer (M = Co, Fe, and Mn) was measured as a function of temperature upon cooling in different applied magnetic fields, and the corresponding magnetic susceptibility (χ_M) and effective magnetic moment ($\mu_{eff} = 2.828\sqrt{\chi_M T}$) were determined.

Figure 5A shows the temperature dependence of the effective magnetic moment determined for Co(μ-$OH_2)_2$[$Au(CN)_2]_2$. At 300 K, the effective moment has a value of ~5.0 μ_B, irrespective of the applied magnetic field. This value is larger than the expected value for a spin-only $S = 3/2$ system (3.87 μ_B) but falls in the range of values usually observed for high-spin Co(II) centers in an octahedral

(29) Korendovych, I. V.; Kryatov, S. V.; Reiff, W. M.; Rybak-Akimova, E. V. *Inorg. Chem.* **2005**, *44*, 8656–8658.

(30) (a) Bancroft, G. M. *Mössbauer Spectroscopy - An introduction for inorganic chemists and geochemists*; McGraw-Hill Book Company Limited: United Kingdom, 1973. (b) Gütlich, P.; Link, R.; Trautwein, A. *Mössbauer Spectroscopy and transition metal chemistry*; Springer-Verlag: New York, 1978.

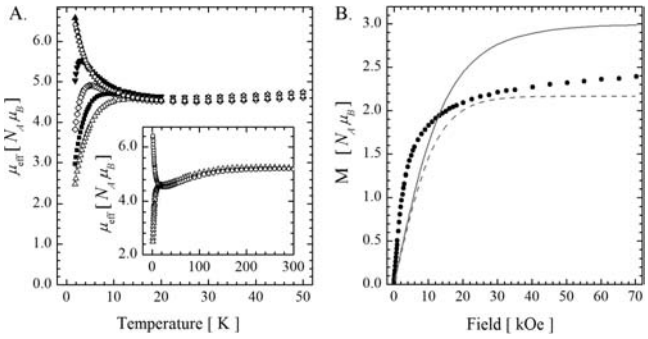

Figure 5. (A) Temperature dependence of the effective magnetic moment (μ_{eff}) of Co(μ-OH_2)$_2$[Au(CN)$_2$]$_2$ measured in a 0.1 (▲), 1 (○), 5 (▼), 10 (◇), 20 (■), and 30 kOe (Δ) field. (B) Field dependence of the magnetization of Co(μ-OH_2)$_2$[Au(CN)$_2$]$_2$ (●) at 1.8 K compared with the Brillouin function (eq S1) for an $S = 3/2$ ($g = 2$, solid line) and for an $S = 1/2$ ($g = 13/3$, dashed line) paramagnetic system.

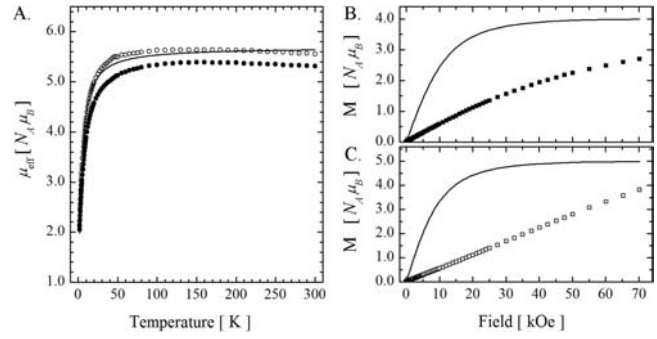

Figure 6. (A) Temperature dependence of the effective magnetic moment (μ_{eff}) of Fe(μ-OH_2)$_2$[Au(CN)$_2$]$_2$ (●) and Mn(μ-OH_2)$_2$[Au(CN)$_2$]$_2$ (○) measured in a 1 kOe dc field; the solid line corresponds to the fit to eq 1 for the Mn-containing polymer. Field dependence of the magnetization of (B) Fe(μ-OH_2)$_2$[Au(CN)$_2$]$_2$ (■) and (C) Mn(μ-OH_2)$_2$[Au(CN)$_2$]$_2$ (□) at 1.8 K compared with the corresponding Brillouin function (solid lines, eq S1) for an $S = 2$ and $S = 5/2$ paramagnetic system, respectively.

environment (4.7−5.2 μ_B), for which spin−orbit coupling is important.[17,28]

Between 300 and 25 K, the effective magnetic moment is nearly field-independent, and a slow decrease with decreasing temperature is observed (inset, Figure 5A). At 25 K, values of 4.5−4.6 μ_B are observed. Below 25 K, the effective moment determined in fields of 100 Oe and 1 kOe increases steadily to reach a value of 6.58 and 6.42 μ_B at 1.8 K, respectively. When the sample is cooled in a field of 5 kOe or more, the effective moment also increases below 25 K, but it reaches a maximum and then decreases. The temperature at which a maximum occurs is field-dependent: the maximum occurs at 3.0, 5.5, and 9.0 K respectively in a magnetic field of 5, 10, and 20 kOe. When a field of 30 kOe is applied, the effective moment remains stable between 25 and 15 K and then drops to reach a value of 2.48 μ_B at 1.8 K.

The different results obtained below 25 K suggest a field-dependent magnetic state. The increase in the effective moment with decreasing temperature at 100 and 1000 Oe indicates the presence of ferromagnetic interactions between the Co(II) centers. The maximum observed in fields of 5 kOe or more suggest that, under these conditions, secondary, weaker magnetic interactions are overcome (see discussion below). At these higher fields, the moments are fully aligned, and thus, the susceptibility saturates, leading to a maximum in the observed effective moment. This behavior is similar to that observed for the analogous Ni(II)-containing polymer, but shifted toward lower temperatures.[7] For example, the Ni(μ-OH_2)$_2$[Au(CN)$_2$]$_2$ polymer showed a maximum in effective moment at 6.4 K in a field of 10 kOe.

The alternating current (ac) susceptibility of Co(μ-OH_2)$_2$[Au(CN)$_2$]$_2$ was also determined as a function of the temperature (in a zero dc field). No nonzero out-of-phase component (χ_M'') and no frequency dependence were observed over the temperature range studied. This behavior differs from that of Ni(μ-OH_2)$_2$[Au(CN)$_2$]$_2$ for which an out-of-phase component (χ_M'') and a frequency dependence were observed below 2.5 K.

The isothermal magnetization determined at 1.8 K for Co(μ-OH_2)$_2$[Au(CN)$_2$]$_2$, as the field is increased from 0 to 70 kOe, is shown in Figure 5B. A rapid increase between 0 and 10 kOe can be seen, followed by a slower increase to reach a value of 2.39 μ_B at 70 kOe. A comparison is made with the spin-only behavior for a paramagnetic $S = 3/2$ ($g = 2$) system following the Brillouin function (eq S1). Due to a combination of spin−orbit coupling and a trigonal distortion to the crystal field, it has been shown that, in the closely related $CoCl_2$ salt, an effective $S = 1/2$ with a g value of ∼13/3 is observed at low temperatures.[31] The calculated magnetization using these values is also shown in Figure 5B. The faster increase of the observed magnetization in the small-field ($H < \sim 8$ kOe) region, compared to both the $S = 1/2$ and 3/2 calculated magnetizations, is consistent with the presence of ferromagnetic interactions in Co(μ-OH_2)$_2$[Au(CN)$_2$]$_2$. The high-field ($H > \sim 10$ kOe) experimental magnetization lies somewhere between the saturation magnetizations M_S expected for a spin-only $S = 3/2$ ($M_S = 3\ \mu_B$) and the spin−orbit coupled $S = 1/2$ case ($M_S = 2.17\ \mu_B$). While the measured value is indeed reduced compared to the spin-only saturation magnetization, the effects discussed in ref 31 (in particular the trigonal distortion) are not as pronounced in Co(μ-OH_2)$_2$[Au(CN)$_2$]$_2$. It is also apparent that the magnetization has not saturated even at a field of 70 kOe. The remaining field dependence at larger fields suggests that interactions are preventing complete spin alignment.

The temperature dependence of the effective magnetic moment determined for Fe(μ-OH_2)$_2$[Au(CN)$_2$]$_2$ and Mn(μ-OH_2)$_2$[Au(CN)$_2$]$_2$ is shown in Figure 6A. For both polymers, the observed magnetic behavior was found to be independent of the external field in the 100−5000 Oe range. For the Fe(II) analogue, the effective magnetic moment was found to be relatively stable between 300 and 75 K at a value of 5.3 μ_B. Below 75 K, the effective magnetic moment drops to reach 2.0 μ_B at 1.8 K. Similarly, the effective magnetic moment of Mn(μ-OH_2)$_2$[Au(CN)$_2$]$_2$ has a value of 5.6 μ_B between 300 and 50 K, before dropping to reach 2.1 μ_B at 1.8 K. The high-temperature values are consistent with high-spin Fe(II) and Mn(II) centers.[17] No maximum is observed in the temperature dependence of the magnetic susceptibility for either polymer. The drop in effective magnetic moment in

(31) Lines, M. E. *Phys. Rev.* **1963**, *131*, 546–555.

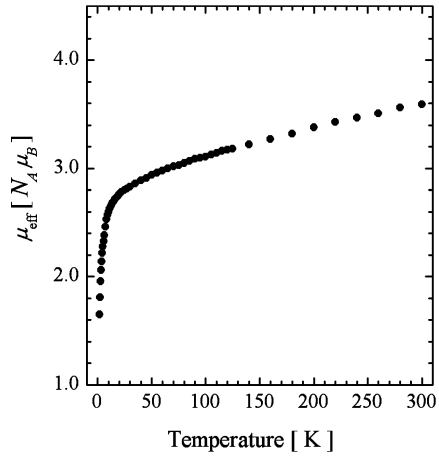

Figure 7. Temperature dependence of the effective magnetic moment (μ_{eff}) of Fe(μ-OH_2)(μ-OH)[$Au(CN)_2$]$_2$ measured in a 10 kOe field.

both polymers suggests the presence of weak antiferromagnetic interactions occurring at low temperatures.

The magnetic susceptibility of Mn(μ-OH_2)$_2$[$Au(CN)_2$]$_2$ was fit to the analytical expression derived by Fisher (eq 1) for an infinite chain of equally spaced classical spins.[32]

$$\chi_{chain} = \frac{N_A g^2 \mu_B^2 S(S+1)}{3k_B T} \times \left(\frac{1+u}{1-u}\right) \quad (1)$$

$$u = \coth\left[\frac{J_{Fisher} S(S+1)}{k_B T}\right] - \left[\frac{k_B T}{J_{Fisher} S(S+1)}\right]$$

In eq 1, J_{Fisher} represents the exchange coupling constant along the chain. The fit to this equation, shown in Figure 6A, yielded a J_{Fisher} value of $-0.33(2)$ cm^{-1} ($g = 1.92(2)$) for Mn(μ-OH_2)$_2$[$Au(CN)_2$]$_2$. This small negative coupling constant also suggests weak antiferromagnetic interactions along the chains. The differences observed between the fit and the experimental data (Figure 6A) are likely due to the presence of interchain interactions, which are not taken into account with this model. The presence of interchain interactions may also be reflected in the g value derived from this analysis, which is lower than that typically expected for a Mn(II) ion.

The isothermal magnetization of the two polymers was determined as a function of the field at 1.8 K. As the field is increased, the magnetization increases steadily to reach 2.69 and 3.8 $N_A\mu_B$ in a field of 70 kOe for the Fe(II)- and Mn(II)-containing polymers, respectively. Figure 6B and C show a comparison between the results obtained experimentally for Fe(μ-OH_2)$_2$[$Au(CN)_2$]$_2$ and Mn(μ-OH_2)$_2$[$Au(CN)_2$]$_2$ and the Brillouin functions (eq S1) for $S = 2$ and $S = 5/2$ paramagnetic systems, respectively. The differences observed between the expected behavior and the experimental data suggest that the Fe(II)- and Mn(II)-containing polymers are not in a paramagnetic state at 1.8 K. The smaller magnetization over the field range studied is also consistent with the presence of antiferromagnetic interactions between the M(II) centers at 1.8 K.

The temperature-dependent magnetic behavior determined for Fe(μ-OH_2)(μ-OH)[$Au(CN)_2$]$_2$ is shown in Figure 7. At 300 K, the effective moment has a value of 3.59 μ_B, which drops steadily upon cooling until 20 K (2.76 μ_B). Below that temperature, a steeper drop in effective moment occurs, and a final value of 1.65 μ_B was determined at 2.0 K. No maximum could be observed in the temperature dependence of the susceptibility. The value observed at room temperature is much smaller than the expected value for an $S = 5/2$ paramagnetic system. This value, along with the continuous decrease in effective magnetic moment, indicates the presence of antiferromagnetic interactions between the Fe(III) centers in Fe(μ-OH_2)(μ-OH)[$Au(CN)_2$]$_2$.

***μ*SR Results.** ZF-μSR experiments were performed for the M(μ-OH_2)$_2$[$Au(CN)_2$]$_2$ (M = Co(II), Fe(II), and Mn(II)) and Fe(μ-OH_2)(μ-OH)[$Au(CN)_2$]$_2$ coordination polymers. The ZF-μSR asymmetry spectra $A(t)$ for each polycrystalline sample were analyzed as the sum of two components:

$$A(t) = a_s P_z(t) + a_{Ag} \quad (1a)$$

where the first term describes the contribution to the signal from muons stopping in the sample, whereas the second term originates from muons stopping in a silver (Ag) backing plate. Because Ag does not contain electronic moments, this background term is independent of both time and temperature.

In all samples, a broad static internal magnetic field distribution develops below a spin-freezing transition temperature T_F. Above T_F, the polarization function $P_z(t)$ is well described by the sum of two exponential relaxation functions:

$$P_z(t) = \frac{1}{2} e^{-\lambda_1 t} + \frac{1}{2} e^{-\lambda_2 t} \quad (2)$$

The two terms correspond to two magnetically inequivalent muon stopping sites having the same site occupancy. The exponential relaxation for each of these muon sites is characteristic of rapid fluctuations of the internal magnetic field in a paramagnetic phase. In zero field, the relaxation rate λ_i ($i = 1, 2$) is inversely proportional to the fluctuation rate ν_i of the internal magnetic field, such that $\lambda_i = 2\gamma_\mu B_i^2/\nu_i$, where B_i is the root-mean-square internal magnetic field at site i and $\gamma_\mu = 0.0852\ \mu s^{-1}\ G^{-1}$ is the muon gyromagnetic ratio.[33]

Below T_F, the polarization function $P_z(t)$ can be described by the following function:

$$P_z(t) = \frac{1}{2}\left(\frac{1}{3} e^{-\lambda_1 t} + \frac{2}{3} e^{-\Lambda_1 t}\right) + \frac{1}{2}\left(\frac{1}{3} e^{-\lambda_2 t} + \frac{2}{3} e^{-\Lambda_2 t}\right) \quad (3)$$

The two-component relaxation function that describes each muon site in eq 3 is characteristic of a highly disordered magnetic state in which the local magnetic field is quasi-static on the microsecond time scale of the muon lifetime. The 1/3 and 2/3 components refer to the probability, for a

(32) Fisher, M. E. *Am. J. Phys* **1964**, *32*, 343–346.

(33) Lee, S. L.; Kilcoyne, S. H.; Cywinski, R. *Muon Science: Muons in Physics, Chemistry and Materials*; Institute of Physics Publishing: Bristol, U.K., 1999.

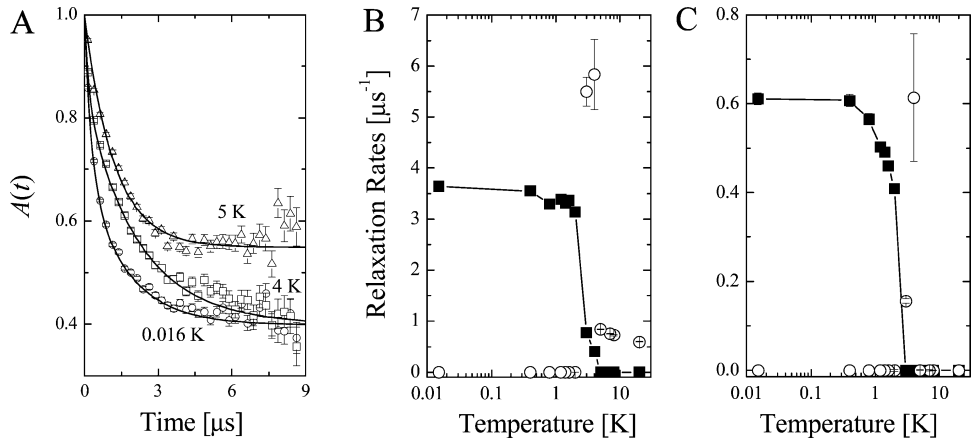

Figure 8. (A) Representative ZF-μSR spectra for Co(μ-OH$_2$)$_2$[Au(CN)$_2$]$_2$ at different temperatures. Lines are fit to eqs 1−3. (B) Temperature dependence of the relaxation rates λ_1 (○) and Λ_1 (■) at muon site 1. (C) Temperature dependence of the relaxation rates λ_2 (○) and Λ_2 (■) at muon site 2. (For B and C, the lines are guides for the eyes.)

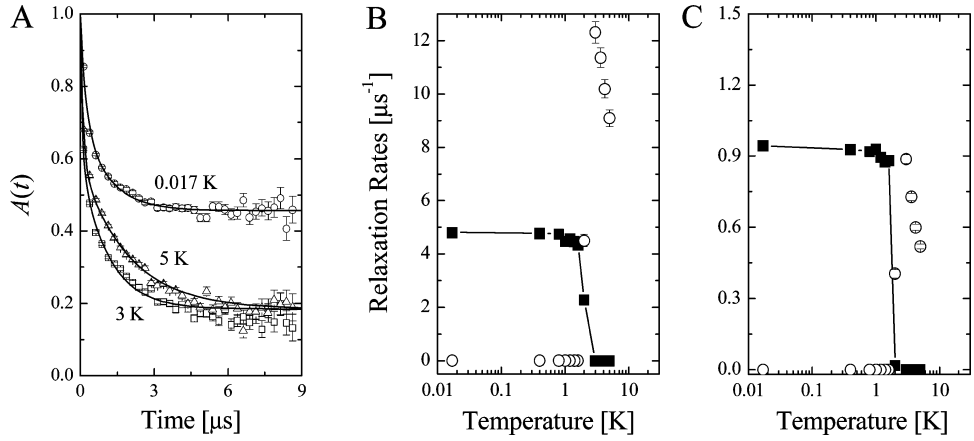

Figure 9. (A) Representative ZF-μSR spectra for Fe(μ-OH$_2$)(μ-OH)[Au(CN)$_2$]$_2$ at different temperatures. Lines are fit to eqs 1−3. (B) Temperature dependence of the relaxation rates λ_1 (○) and Λ_1 (■) at muon site 1. (C) Temperature dependence of the relaxation rates λ_2 (○) and Λ_2 (■) at muon site 2. (For B and C, lines are guides for the eyes.)

polycrystalline sample, that the local magnetic field is either parallel or transverse to the muon spin direction. The exponential relaxation rate Λ_i of the 2/3 component for each muon site corresponds to the width of a local quasi-static Lorentzian magnetic field distribution. The full-width-at-half-maximum of the local field distribution is $2\Lambda_i/\gamma_\mu$. When $\lambda_i = 0$ in eq 3, the internal magnetic field distribution is completely static. We note that a static Lorentzian field distribution is typical of a dilute spin system, which is not really the case here. Consequently, we ascribe the exponential relaxation rates Λ_1 and Λ_2 to a broad range of magnetically inequivalent muon sites surrounding two central muon stopping sites.

Figure 8 shows the results of fits of the ZF-μSR spectra for Co(μ-OH$_2$)$_2$[Au(CN)$_2$]$_2$. The critical divergence of the dynamic relaxation rate λ_i at both muon sites indicates a magnetic transition near $T_F \sim 3.5$ K. We note that, when long-range magnetic order is present, oscillations in the ZF-μSR spectrum are observed, as was reported for Cu(μ-OH$_2$)$_2$[Au(CN)$_2$]$_2$ below $T \sim 0.24$ K.[7] As shown in Figure 8A, no oscillations were observed for Co(μ-OH$_2$)$_2$[Au(CN)$_2$]$_2$, even at the lowest temperature reached ($T = 0.016$ K). Instead, the abrupt increase of Λ_1 and Λ_2 below T_F and the saturation of these quantities with decreasing temperature indicate that the spins freeze into a highly disordered state. As shown in Figure 9, similar results were obtained for Fe(μ-OH$_2$)(μ-OH)[Au(CN)$_2$]$_2$, with a spin-freezing transition occurring near $T_F \sim 3$ K.

As shown in Figure 10A, the initial relaxation of the ZF-μSR spectra for Mn(μ-OH$_2$)$_2$[Au(CN)$_2$]$_2$ is so fast that the early part of the spectrum is lost in the initial dead time (~10 ns) of the μSR spectrometer even above the spin freezing temperature 2 K < T_F < 5 K. Figure S5 (Supporting Information) shows that below T_F some of the asymmetry is recovered by the application of a 1 kOe longitudinal field. There are, however, large static internal fields sensed by the muons, which are responsible for the fast relaxation still observed at 1 kOe. The nonrelaxing component of both the ZF-μSR and LF-μSR spectra, clearly visible at late times, indicates that the internal fields are quasi-static below T_F. The larger value of λ_1 above T_F (Figure 10B) indicates a much slower spin fluctuation rate in the paramagnetic phase compared to Co(μ-OH$_2$)$_2$[Au(CN)$_2$]$_2$ and Fe(μ-OH$_2$)(μ-OH)[Au(CN)$_2$]$_2$. While the temperature dependence of λ_2 for Mn(μ-OH$_2$)$_2$[Au(CN)$_2$]$_2$ (Figure 10C) qualitatively resembles that of λ_1, its magnitude is comparable to those of the other samples (Figures 8C and 9C). It is likely then that site 1 is closer to the metal-center chains than site 2, so that a muon

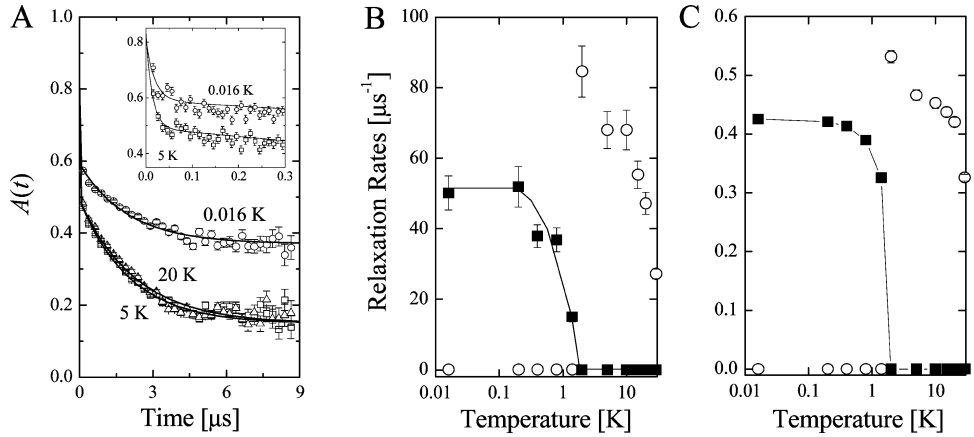

Figure 10. (A) Representative ZF-μSR spectra for $Mn(\mu\text{-}OH_2)_2[Au(CN)_2]_2$ at different temperatures. The inset shows the fast relaxation of the ZF-μSR spectra at early times. Lines are fit to eqs 1−3. (B) Temperature dependence of the relaxation rates λ_1 (○) and Λ_1 (■) at muon site 1. (C) Temperature dependence of the relaxation rates λ_2 (○) and Λ_2 (■) at muon site 2 (For B and C, lines are guides for the eyes.).

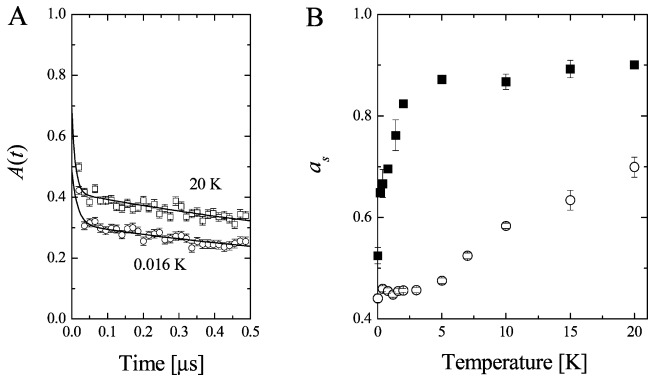

Figure 11. (A) Representative ZF-μSR spectra for $Fe(\mu\text{-}OH_2)_2[Au(CN)_2]_2$ at different temperatures. Lines are fit to eqs 1−3. (B) Temperature dependence of the initial sample asymmetry of $Fe(\mu\text{-}OH_2)_2[Au(CN)_2]_2$ (○) and $Mn(\mu\text{-}OH_2)_2[Au(CN)_2]_2$ (■).

at site 1 senses a larger root-mean-square internal magnetic field from the buildup of intrachain magnetic interactions with decreasing temperature. Consistent with this assertion is the very broad local field distribution detected at site 1 in the spin-frozen state. In particular, below T_F the static relaxation rate Λ_1 for $Mn(\mu\text{-}OH_2)_2[Au(CN)_2]_2$ ($\Lambda_1 \sim 55\ \mu s^{-1}$) is an order of magnitude larger than in $Co(\mu\text{-}OH_2)_2[Au(CN)_2]_2$ and $Fe(\mu\text{-}OH_2)(\mu\text{-}OH)[Au(CN)_2]_2$ ($\Lambda_1 \sim 3.5-5\ \mu s^{-1}$), whereas Λ_2 is comparable ($\Lambda_2 \sim 0.4-0.6\ \mu s^{-1}$).

Similar ZF-μSR spectra were obtained from measurements on $Fe(\mu\text{-}OH_2)_2[Au(CN)_2]_2$ (Figure 11A). However, in the case of $Fe(\mu\text{-}OH_2)_2[Au(CN)_2]_2$, the initial asymmetry is reduced so much at low temperatures that the spectra cannot be fit over the entire temperature range with a common value for a_s. Figure 11B shows the temperature dependence of the initial sample asymmetry for $Fe(\mu\text{-}OH_2)_2[Au(CN)_2]_2$ and $Mn(\mu\text{-}OH_2)_2[Au(CN)_2]_2$ determined from fits of the ZF-μSR spectra over the first 0.5 μs (Figure 10A inset and Figure 11A). The freezing transition for $Mn(\mu\text{-}OH_2)_2[Au(CN)_2]_2$ is indicated by an abrupt drop of a_s. Compared to $Mn(\mu\text{-}OH_2)_2[Au(CN)_2]_2$, the initial asymmetry of $Fe(\mu\text{-}OH_2)_2[Au(CN)_2]_2$ above T_F is considerably smaller, indicating that the spin fluctuations in the paramagnetic phase are even slower. The saturation of a_s at low temperatures suggests that there is a spin-freezing transition at a temperature comparable to that for the other samples, giving rise to an internal field distribution that is so broad that the initial relaxation is too fast to be observed.

Discussion

Multiple Magnetic Pathways and Spin Frustration. Spin frustration arises from the competition or contradictory constraints imposed by various magnetic pathways on a given spin center.[34] For example, in a triangular geometry where the interactions between the three spin centers favor antiferromagnetic alignment, it will be impossible for every site to accommodate both antiferromagnetic interactions with its two neighbors, and the system will be spin-frustrated.

As we have previously described for the analogous Cu(II)- and Ni(II)-containing polymers,[7] magnetic exchange between the metal centers in $M(\mu\text{-}OH_2)_2[Au(CN)_2]_2$ can occur through several pathways. The pathways believed to be predominant are shown in Scheme 1. In this discussion, the exchange constant J_i refers to the Heisenberg Hamiltonian, $H = -J_{AB}\mathbf{S_A}\cdot\mathbf{S_B}$, which makes no assumptions about the microscopic origin of the coupling.

The interactions mediated through the short double aqua bridges $M(\mu\text{-}OH_2)_2M$ (J_1) are most likely the strongest interactions in every polymer studied here. Magnetic interchain interactions are also possible, either through M−OH···N···HO−M (J_2) or M−OH···NCAuCN−M (J_3). These pathways, which involve hydrogen-bonding interactions between the $[Au(CN)_2]^-$ units and the water molecules, likely mediate weaker interactions due to the longer distances involved. Both of these building blocks were previously shown to mediate magnetic exchange in different systems.[7,35] Notice that this magnetic structure model leads to the existence of two triangular magnetic sublattices in the M(μ-

(34) Greedan, J. E. *J. Mater. Chem.* **2001**, *11*, 37–53.
(35) (a) Leznoff, D. B.; Xue, B.-Y.; Patrick, B. O.; Sanchez, V.; Thompson, R. C. *Chem. Commun.* **2001**, 259–260. (b) Leznoff, D. B.; Xue, B.-Y.; Batchelor, R. J.; Einstein, F. W. B.; Patrick, B. O. *Inorg. Chem.* **2001**, *40*, 6026–6034. (c) Plass, W.; Pohlmann, A.; Rautengarten, J. *Angew. Chem., Int. Ed.* **2001**, *40*, 4207–4210. (d) Ardon, M.; Bino, A.; Michelsen, K.; Pedersen, E.; Thompson, R. C. *Inorg. Chem.* **1997**, *36*, 4147–4150. (e) Rancurel, C.; Daro, N.; Benedi Borobia, O.; Herdtweck, E.; Sutter, J.-P. *Eur. J. Org. Chem.* **2003**, 167–171. (f) Luneau, D.; Rey, P.; Laugier, J.; Belorizky, E.; Cogne, A. *Inorg. Chem.* **1992**, *31*, 3578–3584.

Scheme 1. Possible Magnetic Pathways in $M(\mu\text{-}OH_2)_2[Au(CN)_2]_2$[a]

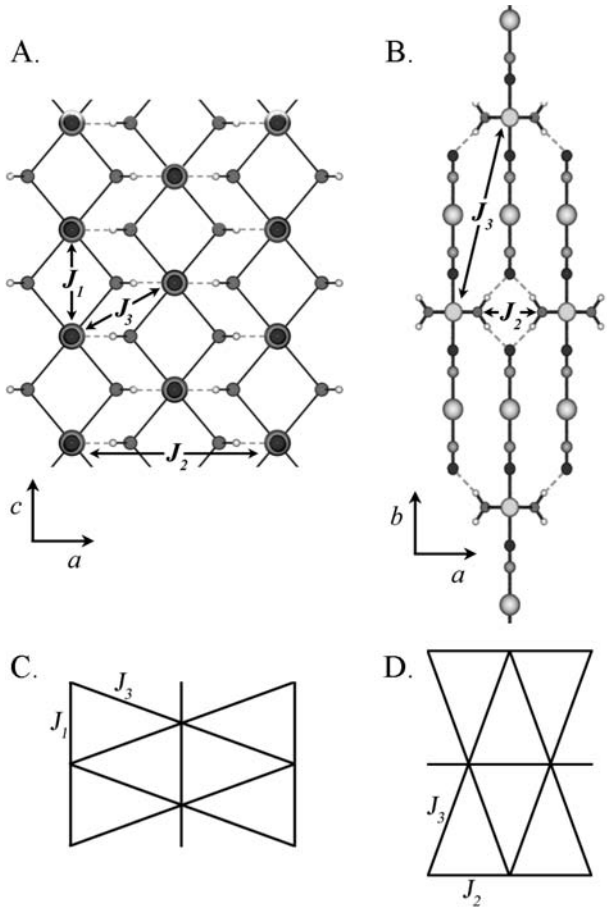

[a] Interactions along the $M(\mu\text{-}OH_2)_2M$ chains (J_1) and interchain interactions (J_2, J_3). (A) Structure viewed down the *b* axis and (B) viewed down the chain axis. Dotted lines indicate hydrogen bonding. Triangular magnetic sublattices containing the J_1 and J_3 (C) and the J_2 and J_3 (D) coupling constants.

$OH_2)_2[Au(CN)_2]_2$ compounds. The first is composed of isosceles triangles, where one side is described by J_1 and the two equivalent sides by J_3 (Scheme 1C), and lies within the [110] plane. The second sublattice also consists of isosceles triangles, with sides J_2 and J_3 (Scheme 1D), and lies in the [011] plane. This corresponds to M−M distances, for example for M = Co, ranging from intrachain 3.388 Å to interchain 6.40, 7.24, and 10.92 (average) Å.

One-dimensional magnetic chain complexes have a long history; chains with metal centers bridged by halides are particularly widespread.[36] In general, in addition to the primary intrachain coupling, the weaker interactions between chains are always a critical factor in determining the overall magnetic properties. Of particular relevance to the work here is the case of $MCl_2 \cdot 2H_2O$ (M = Co, Ni), which contains chains of metal(II) ions bridged by chloride ions and for which a similar coupling scheme to that proposed for $M(\mu\text{-}OH_2)_2[Au(CN)_2]_2$ was utilized.[37] Thus, the strongest interactions in $MCl_2 \cdot 2H_2O$ are mediated along the halide-bridged chains (for M = Co, the intrachain coupling is also ferromagnetic). Weaker (antiferromagnetic) interchain interactions are mediated through Co−Cl···Cl−Co pathways, with a Co···Co distance of nearly 9 Å. Although the interchain interactions are weaker, they are responsible for the long-range order observed below 17.5 K in $CoCl_2 \cdot 2H_2O$.[37] There are both longer and shorter interchain M−M distances along the magnetic pathways in the $M(\mu\text{-}OH_2)_2[Au(CN)_2]_2$ coordination polymers (see previous paragraph) compared to $CoCl_2 \cdot 2H_2O$, and this combination could help account for the significantly lower transition temperatures in the $M(\mu\text{-}OH_2)_2[Au(CN)_2]_2$ system (17.5 K vs 2−5 K).

The type and strength of interactions mediated by the aqua bridge depends on the extent of overlap between the magnetic orbitals of the metal centers and the orbitals of the oxygen atoms;[17] this, in turn, depends on the structural arrangement. The differences between the magnetic behavior observed for each $M(\mu\text{-}OH_2)_2[Au(CN)_2]_2$ and $Fe(\mu\text{-}OH_2)(\mu\text{-}OH)[Au(CN)_2]_2$ polymer arise mainly from (1) the slight structural differences in the double aqua bridges (distances, angles, asymmetric vs symmetric motif), (2) the differences in the metal centers' geometry (highly symmetrical vs distorted), and (3) the number of unpaired electrons (one to five unpaired electrons for Cu(II) to Mn(II)) and their associated magnetic orbitals.

Magnetic Exchange through Double Aqua Bridges (J_1). As was presented in the Results section, ferromagnetic interactions dominate the observed magnetic properties in $Co(\mu\text{-}OH_2)_2[Au(CN)_2]_2$ (Figure 5), and we suggest that these interactions are mediated between the Co(II) centers through the double aqua bridges; that is to say, J_1 has a positive value. This is similar to the magnetic behavior observed for $Ni(\mu\text{-}OH_2)_2[Au(CN)_2]_2$.[7] The temperature dependence of the effective magnetic moment for the Co(II)-containing polymer (Figure 5) is shifted toward a lower temperature compared to the behavior of the Ni(II) analogue, suggesting weaker intrachain interactions in the Co(II) system. On the other hand, the magnetic behavior of the Fe(II)- and Mn(II)-containing $M(\mu\text{-}OH_2)_2[Au(CN)_2]_2$ polymers differ greatly from that of Co(II) (c.f., Figure 6), and this suggests that antiferromagnetic intrachain interactions ($J_1 < 0$) are present at low temperatures.

An increase in the M−M distance was observed when going from the Ni(II) structure (3.3183(11) Å)[7] to the Co(II) (3.388 Å), Fe(II) (3.465 Å), and Mn(II) (3.49 Å) structures, which can be attributed in part to an increase in atomic radii. In addition, larger M−M distances can impose larger M−O−M angles, unless there is a large increase in M−O distances. However, as mentioned earlier, the positions of the oxygen atoms could not be determined with precision for most $M(\mu\text{-}OH_2)_2[Au(CN)_2]_2$ polymers, and no quantitative structural comparison can therefore be made to explain the different interactions. The M−O−M angle most likely varies among the different $M(\mu\text{-}OH_2)_2[Au(CN)_2]_2$ polymers. In several other oxygen-bridged systems, larger M−O−M angles are usually associated with the mediation of antifer-

(36) (a) de Jongh, L. J.; Miedema, A. R. *Adv. Phys.* **1974**, *23*, 1–260. (b) Steiner, M.; Villain, J.; Windsor, C. G. *Adv. Phys.* **1976**, *25*, 87–209. (c) Hatfield, W. E.; Estes, W. E.; Marsh, W. E.; Pickens, M. W.; ter Haar, L. W.; Weller, R. R. In *Extended Linear Chain Compounds*; Miller, J. S., Ed.; Plenum Press: New York, 1983; p 43.
(37) Narath, A. *Phys. Rev.* **1964**, *136*, A766–A771.

Table 2. Comparison between the Magnetic Behavior of the Different $M(\mu\text{-}OH_2)_2[Au(CN)_2]_2$ and $Fe(\mu\text{-}OH_2)(\mu\text{-}OH)[Au(CN)_2]_2$ Polymers

		intrachain interactions	interchain interactions		magnetic transitions	
metal centers	S	J_1	J_2	J_3	spin state	transition temperature
Cu(II)[a]	1/2	>0 0.37(2) cm^{-1}	>0	≠ 0	long-range order	T_N = 0.20 K
Ni(II)[a]	2/2	>0	<0	≠ 0	spin-glass	T_F= 3.5 K
Co(II)	3/2	>0	<0	≠ 0 very weak coupling	spin-frozen highly correlated	3 K < T_F < 4.0 K
Fe(II)	4/2	<0		≠ 0 considerable coupling	spin-frozen lower correlation	T_F < 5 K
Mn(II)	5/2	<0 −0.33(2) cm^{-1}		≠ 0 considerable coupling	spin-frozen lower correlation	2 K < T_F < 5 K
Fe(III)	5/2	<0		--[b]	spin-frozen highly correlated	2 K < T_F < 3 K

[a] From ref 7. [b] This pathway differs in the $Fe(\mu\text{-}OH_2)(\mu\text{-}OH)[Au(CN)_2]_2$ structure.

Scheme 2. Schematic Representation of the Magnetic Interchain Interactions Leading to Different Magnetic Ground States[a]

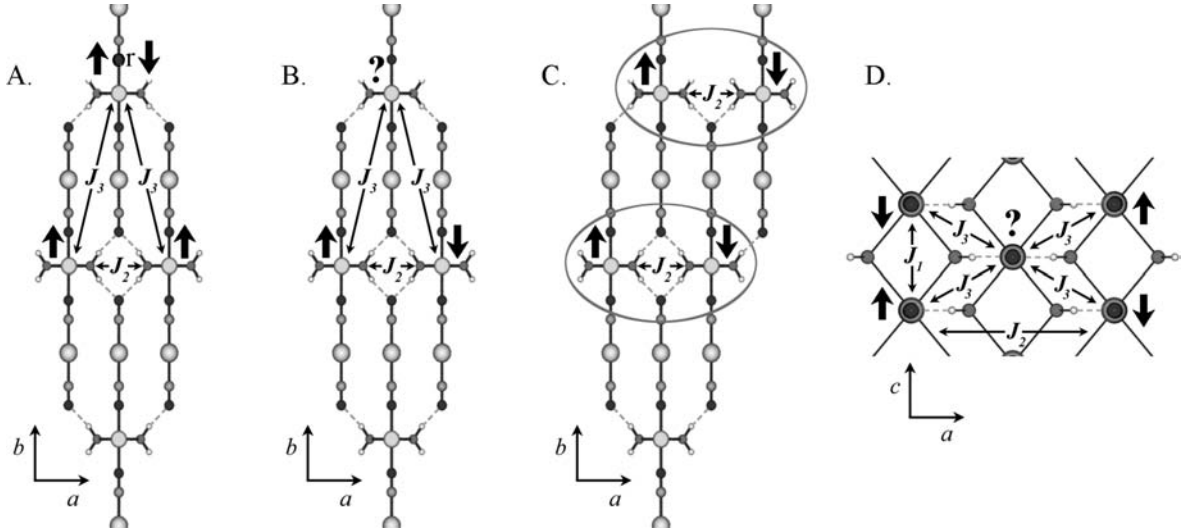

[a] (A) Long-range order in $Cu(\mu\text{-}OH_2)_2[Au(CN)_2]_2$ ($J_2 > 0$). (B) A disordered spin-frozen state in the intrachain ferromagnetically ($J_1 > 0$) coupled Ni- and Co-containing polymers, which results from a negative J_2 coupling constant. (C) For a very large J_2/J_3 ratio, interactions along J_2 dominate. (D) Magnetic interactions in the intrachain antiferromagnetically coupled ($J_1 < 0$) $Fe(\mu\text{-}OH_2)(\mu\text{-}OH)[Au(CN)_2]_2$ and Fe(II)- and Mn(II)-containing $M(\mu\text{-}OH_2)_2[Au(CN)_2]_2$ polymers.

romagnetic interactions, whereas smaller angles mediate ferromagnetic interactions.[10] The change in angle could allow more orbital overlap via the oxygen atom and cause stronger antiferromagnetic interactions between the metal centers.

The magnetic data reported for the few known doubly aqua-bridged Fe(II) and Mn(II) dimers also indicated that very weak antiferromagnetic interactions were mediated through these bridges.[22,24,25] The reported coupling constants for these complexes range between −0.02 and −1.38 cm^{-1} (with the M−O−M angle varying between 100 and 113°). These coupling constants are on the same order of magnitude as the value obtained for the $Mn(\mu\text{-}OH_2)_2[Au(CN)_2]_2$ polymer using the Fisher expression ($J_1' J_{Fisher} = -0.33(2)$ cm^{-1}, eq 1).

Importance of Weak Interchain Interactions (J_2 and J_3). To explain the spin freezing transition observed by ZF-μSR for every $M(\mu\text{-}OH_2)_2[Au(CN)_2]_2$ polymer, interchain magnetic interactions must be present. Table 2 and Scheme 2 summarize the observed magnetic behavior and the magnetic models that are proposed below for the different $M(\mu\text{-}OH_2)_2[Au(CN)_2]_2$ polymers.

In the Co(II)-containing system, a negative J_2 coupling constant can explain the frozen disordered state observed by ZF-μSR below 3.5 K (Figure 8). As shown in Scheme 2B, spin frustration results from competing interactions when J_2 is negative and J_3 has a non-negligible value, whether positive or negative. As a result, a frozen disordered magnetic state is obtained below a critical temperature, which depends on the magnitude of the competing coupling constants. The same type of interchain magnetic interaction ($J_2 < 0$) was also proposed to be present in the analogous $Ni(\mu\text{-}OH_2)_2[Au(CN)_2]_2$ coordination polymer, which also undergoes a spin-freezing transition to a disordered state.[7]

For the Ni(II)-containing polymer, in addition to the maximum observed in the effective magnetic moment, a maximum in magnetic susceptibility was observed below 2 K by SQUID magnetometry.[7] This maximum was attributed to the presence of antiferromagnetic interactions/spin frustration occurring between the chains, consistent with a negative J_2 coupling constant. For the Co(II) analogue, no maximum in magnetic susceptibility was observed above 1.8 K, which could suggest that the interchain interactions are weaker in this system.

Magnetic frustration in the J_2-J_3 plane is likely to affect the spin alignment along the chain. Below the freezing temperature, the relaxation rate Λ of the ZF-μSR spectrum

for the Ni(II)-containing system is considerably larger ($\sim$18 μs^{-1}) than that observed for the Co(II)-containing system ($\Lambda_1 = 3.7\ \mu s^{-1}$, Figure 8B). This difference can be explained by a higher degree of spin correlation along the chains in the Co(II)-containing polymer. Assuming the same type of magnetic exchange in both systems, a larger J_2/J_3 ratio in Co(μ-OH_2)$_2$[Au(CN)$_2$]$_2$, due to either a stronger J_2 or weaker J_3 coupling constant, could explain the higher degree of spin correlation observed by ZF-μSR. As shown in Scheme 2C, for very large J_2/J_3 ratios, the systems could be represented simply as isolated layers of antiferromagnetically coupled chains in which spin frustration is not present.

Despite the presence of ferromagnetic interactions along the chain ($J_1 > 0$), the Cu(II)-containing system studied previously differs from the Co(II) and Ni(II) analogues in that long-range magnetic order is present at low temperatures.[7] In this system, a positive J_2 coupling constant was proposed to be present with a nonzero J_3 constant, which could either be positive or negative (Scheme 2A). Ferromagnetic alignment along the J_2 pathway could result from the presence of only one magnetic orbital per Cu(II) center.

For the polymers in which the intrachain interactions, J_1, are antiferromagnetic (e.g., Fe(II) and Mn(II)), a transition to an even more disordered frozen magnetic state was observed by ZF-μSR. Also, compared to the systems in which ferromagnetic intrachain interactions are present, the spin dynamics were determined to be very slow in the Mn(II)- and Fe(II)-containing systems even above the freezing temperature (in the paramagnetic phase), as evidenced by the large λ_1 and λ_2 relaxation rates (Figure 10B and C).

As is shown in Scheme 2D, when antiferromagnetic coupling is present along the chains ($J_1 < 0$), any interactions between the chains through the J_3 pathway would lead to magnetic frustration, irrespective of the sign or magnitude of J_2. It is suggested that, similar to the Ni(II)- and Co(II)-containing systems, magnetic exchange through the J_2 pathway is also antiferromagnetic in the Fe(II) and Mn(II) systems. In addition to the J_2/J_3 ratio, the J_1/J_3 ratio is also important in these systems. For a large J_1/J_3 ratio, the antiferromagnetically coupled chains can be considered almost isolated. However, as J_1/J_3 decreases (due to a larger J_3), magnetic competitions and frustration increase.

The very large ZF-μSR relaxation rate associated with muons stopping close to the chains (site 1, Λ_1) in Mn(μ-OH_2)$_2$[Au(CN)$_2$]$_2$ (Figure 10B) is consistent with a high degree of magnetic disorder along the chains, which likely results from interchain frustration. A highly disordered state is also present in the Fe(II)-containing system, causing a complete loss of the early time ZF-μSR signal (Figure 11). The field-dependent magnetization of the Fe(II)- and Mn(II)-containing systems (Figure 6) at 1.8 K are also consistent with frozen disordered systems in which a large energy barrier needs to be overcome to align all of the magnetic moments with the external magnetic field. The stronger interchain magnetic interactions in the Fe(II)- and Mn(II)-containing systems could be explained by the larger number of magnetic orbitals participating in the magnetic exchange.

Magnetic Exchange through Aqua and Hydroxide Bridges. The magnetic properties observed for the structurally related Fe(μ-OH_2)(μ-OH)[Au(CN)$_2$]$_2$ polymer also suggest that antiferromagnetic interactions are mediated along the shortest J_1 magnetic pathway. The nature of this pathway however differs in Fe(μ-OH_2)(μ-OH)[Au(CN)$_2$]$_2$ and could consist of either alternating double aqua bridges/double hydroxide bridges or mixed aqua-hydroxide bridges.

Very few examples of aqua-hydroxide bridged complexes are known, and the magnetic behavior of most of them has not been investigated. In the aqua-hydroxide bridged high-spin Fe(II) dimer, [Fe$_2$(μ-OH_2)(μ-OH)(TPA)$_2$]$^{3+}$ (TPA = tris(picolylamine)), antiferromagnetic interactions were determined to be present through this mixed bridge, with a coupling constant of -9.6 cm^{-1}.[29] Despite the differences between this dimer and Fe(μ-OH_2)(μ-OH)[Au(CN)$_2$]$_2$ (including the different S value), it is likely that the aqua-hydroxide bridge mediates similar types of interactions in both systems.

The presence of stronger magnetic interactions in Fe(μ-OH_2)(μ-OH)[Au(CN)$_2$]$_2$, compared to the M(μ-OH_2)$_2$[Au(CN)$_2$]$_2$ polymers, likely results from the hydroxide groups present between the Fe(III) centers. The properties of hydroxide bridges have been widely investigated, especially in Cu(II) dimers, in which they were found to be good mediators of both ferro- and antiferromagnetic interactions with coupling constants ranging from -509 to $+178$ cm^{-1}.[9] For the doubly hydroxide-bridged dimers, the M$-$O$-$M angles as well as the position of the hydrogen atoms with respect to the MO_2M plane (in or out of the plane) were found to be determinant. Small M$-$O$-$M angles and large out-of-plane M$-$O$-$H angles were found to favor strong ferromagnetic interactions in Cu(II) dimers.[10] The presence of double hydroxide bridges, through which metal centers are more strongly coupled, could explain the smaller effective moment observed at room temperature.

It is interesting to notice that aqua bridges are weak mediators of magnetic interactions compared to hydroxide-bridges. Slight structural differences between the two bridges are sometimes observed, with M$-$O distances being slightly shorter in a hydroxide bridge.[29] These structural differences could explain in part the different magnitudes in coupling constants, but other variables such as the molecular orbitals involved and the extent of overlap with those of the metal centers should also be taken into consideration.[17,38] Theoretical calculations would shed further light on this issue.

The structure of the Fe(μ-OH_2)(μ-OH)[Au(CN)$_2$]$_2$ polymer also differs from that of the M(II)-containing polymers due to the crystallographic random half-occupancy of the Fe(III) centers. As a result, the J_3 pathway is not present in all of the unit cells, but only in half of them (Figure 3). This half-occupancy should decrease the overall amount of frustration in the system and, as a result, increase the degree of spin correlation along the chain. This hypothesis is consistent with

(38) Kollmar, C.; Kahn, O. *Acc. Chem. Res.* **1993**, *26*, 259–265.

the much smaller ZF-μSR relaxation rate associated with muons sitting close to the chains in Fe(μ-OH_2)(μ-OH)[$Au(CN)_2$]$_2$ (Figure 9B) compared to Mn(μ-OH_2)$_2$[$Au(CN)_2$]$_2$ (Figure 10B) and presumably Fe(μ-OH_2)$_2$[$Au(CN)_2$]$_2$, although the relaxation rate is so fast in the Fe(II) polymer that different muon sites could not be resolved.

In addition, the structural model for Fe(μ-OH_2)(μ-OH)[$Au(CN)_2$]$_2$ (Figure 3) includes a different bridge between the metal centers, Fe−NCAuCN−Fe. This additional path can mediate magnetic interactions without introducing an element of magnetic frustration in the system. As a result of these structural differences, despite the presence of antiferromagnetic interactions along the chains ($J_1 < 0$), a higher degree of spin correlation is present in the Fe(μ-OH_2)(μ-OH)[$Au(CN)_2$]$_2$ polymer compared to the Fe(II)- and Mn(II)-containing M(μ-OH_2)$_2$[$Au(CN)_2$]$_2$ polymers.

Conclusion

Three new isostructural M(μ-OH_2)$_2$[$Au(CN)_2$]$_2$ (M = Co, Fe, Mn) coordination polymers containing the rare double aqua bridge M(μ-OH_2)$_2$M motif were presented along with the related Fe(μ-OH_2)(μ-OH)[$Au(CN)_2$]$_2$ polymer, in which a water molecule is replaced by a hydroxide group. A complete picture of their magnetic behavior was obtained by combining SQUID magnetometry and ZF-μSR studies in the presence and absence of a magnetic field. This unusual combination of techniques proved to be necessary to fully understand the magnetic ground states.

The double-aqua bridges in these coordination polymers were found to mediate either ferromagnetic or antiferromagnetic interactions between the metal centers depending on their identity. In comparison to the well-studied oxo and hydroxo bridges, these aqua bridges are poor mediators of magnetic exchange, with interactions occurring only at low temperatures, irrespective of the metal centers.

This study illustrates the importance of weak magnetic interactions, and their power to govern the overall magnetic properties. Competition between the weak interchain interactions mediated by hydrogen bonding resulted in the formation of frozen disordered magnetic states in each polymer. The ratios of intra- (J_1) and interchain coupling constants (J_2, J_3) were also found to be important and yielded different degrees of spin correlation for the different polymers.

Acknowledgment. This work was supported by NSERC, TRIUMF, and SFU. The SQUID magnetometer facility was funded by CFI and BCKDF. The authors thank Dr. Brian O. Patrick (University of British Columbia) for measuring the powder diffraction data for the Co-, Mn-, and Fe(III)-containing polymers.

Supporting Information Available: Powder X-ray diffractograms measured and calculated, as well as tables of atomic coordinates for each compound, eq S1, and the LF-μSR data determined for the Mn-containing polymer. This material is available free of charge via the Internet at http://pubs.acs.org.

IC801094M